High Pressure Research
Vol. 28, No. 3, September 2008, 405–413

Taylor & Francis
Taylor & Francis Group

Downloaded By: [Whitaker, Matthew L.][State University of New York at Stony Brook] At: 04:07 28 September 2008

Compressional and shear wave velocities of Fe_2SiO_4 spinel at high pressure and high temperature

Qiong Liu*, Wei Liu, Matthew L. Whitaker, Liping Wang and Baosheng Li

Mineral Physics Institute, Stony Brook University, Stony Brook, NY, USA

(*Received 22 May 2008; final version received 13 June 2008*)

Ultrasonic interferometric measurements on polycrystalline Fe_2SiO_4 spinel were conducted simultaneously with synchrotron X-ray diffraction and X-ray imaging up to 6.5 GPa, 1073 K. The compressional and shear wave velocity data and the volume data were fitted to the third-order finite strain equations to derive the bulk and shear modulus and their pressure and temperature derivatives. The fitting results are as follows: $K_{s0} = 204.5(7)$ GPa, $= 73.6(3)$ GPa, $K_s' = 4.3(3)$, $G' = 1.2(1)$, $(\partial K_s/\partial T)_p = -0.027(2)$ GPa/K, and $(\partial G/\partial T)_p = -0.017(1)$ GPa/K. Comparison of our current results with previous data on $(Mg,Fe)_2SiO_4$ spinel with different compositions suggests that the bulk modulus (K_s) increases slightly with increasing iron content, while the shear modulus (G), in contrast, shows a dramatic decrease. However, the pressure and temperature derivatives of K_s and G remain nearly constant from Mg_2SiO_4 to Fe_2SiO_4 spinel with average values of 4.2–4.4, 1.2–1.3, −0.024 GPa/K, and −0.016 GPa/K for K_s', G', $(\partial K_s/\partial T)_p$, and $(\partial G/\partial T)_p$, respectively. The proposed version of equations to describe the effects of iron on the elastic moduli of ringwoodite are: $K_s = 184.7 + 18.0X_{Fe}$, and $G = 118.7 - 41.5\,X_{Fe}$.

Keywords: ultrasonic interferometry; Fe_2SiO_4 spinel; elastic properties; iron content

1. Introduction

Knowledge of the elastic properties of mantle minerals is essential for the interpretation of seismic data to place constraint on the earth's deep interior. Ringwoodite, $(Mg,Fe)_2SiO_4$, is believed to be the most abundant mineral in the lower part of the mantle transition zone (∼520–660 km). Phase transformations from wadsleyite to ringwoodite and from ringwoodite into $(Mg,Fe)SiO_3$ perovskite and (Mg,Fe)O magnesiowustite are widely accepted to be responsible for the 520 and 660 km discontinuities. Although there is an extensive set of data on the elastic properties of Mg_2SiO_4 spinel [1–8], the elastic data for the iron end-member, Fe_2SiO_4 spinel, are very sparse, especially at simultaneous high temperature and high pressure. Since iron content in mantle $(Mg,Fe)_2SiO_4$ phases varies with depth due to chemical interactions with other mantle phases at high pressure and temperature, it is therefore important to determine the elastic properties of the polymorphs of the Fe_2SiO_4 end-member for a precise modeling of the Mg_2SiO_4–Fe_2SiO_4 system and thus a better understanding of the physics and chemistry of the mantle. Here, we present

*Corresponding author. Email: qioliu@notes.cc.sunysb.edu

ISSN 0895-7959 print/ISSN 1477-2299 online
© 2008 Taylor & Francis
DOI: 10.1080/08957950802296287
http://www.informaworld.com

new results of elastic property measurements on Fe_2SiO_4 spinel simultaneously at high pressure and high temperature (up to 6.5 GPa, 1073 K) using combined ultrasonic interferometry, X-ray diffraction, and X-ray imaging techniques [9]. These data, together with results from previous studies, allow us to explore the dependence of elastic bulk and shear properties on iron content across the Mg_2SiO_4–Fe_2SiO_4 solid solution.

Downloaded By: [Whitaker, Matthew L.][State University of New York at Stony Brook] At: 04:07 28 September 2008

2. Experimental

The starting material of fayalite is synthesized by Donald Lindsley from carefully weighed and ground oxide components in a Fe-saturated Pt crucible at 1373 K for 4 hours in the CO–CO_2 atmosphere maintained at f_{o_2} in the fayalite stability field. The synthesized powder was packed tightly in an iron capsule and hot-pressed at ~5 GPa, 1073 K for 1 hour in a 1000-ton uniaxial split-cylinder apparatus (USCA-1000). The recovered polycrystalline sample, confirmed to be single phase of fayalite by X-ray diffraction at beamline X17B2 of National Synchrotron Light Source (NSLS) in Brookhaven National Laboratory (BNL), was converted to spinel phase during the current ultrasonic experiment conducted in the DDIA-type cubic anvil press (SAM85) installed at X17B2 at BNL. The experimental set-up and the technique of the ultrasonic interferometry are described in detail elsewhere [9]. Briefly, the sample was placed in the center of the boron epoxy cube which was used as pressure transmitting medium, with NaCl and BN mixture (10:1 by weight) as surrounding material to provide a pseudo-hydrostatic pressure environment. Polished alumina rod with flat and parallel surfaces (within 0.05°) was inserted into the pressure medium and used as an acoustic buffer rod.

Ultrasonic data were acquired using the transfer function method [10] with a dual mode lithium niobate transducer (10 degree Y-cut, 30 MHz for S wave and 50 MHz for P wave). A broadband radio-frequency (20–70 MHz) pulse is transmitted and received by the piezoelectric transducer, the round-trip propagation time inside the sample is obtained by measuring the time delay between two consecutive echoes reflected from the front and rear surfaces of the sample (Figure 1). P and S wave travel times were determined simultaneously with one standard deviation of ~0.2 ns and ~0.4 ns, respectively. Sample length was monitored by X-ray radiographic imaging system consisting of an yttrium aluminum garnet (YAG), a mirror, and a charge couple device (CCD) camera [9]. Figure 2 shows an example of the X-ray image of the sample at high pressure. The uncertainty of the sample length with respect to pixel number is ~2–4 pixels, which gives a 0.2–0.4% precision.

Energy-dispersive X-ray diffraction data were collected using a solid-state Ge detector for phase identification, density determination, and pressure calculation. The incident X-ray beam was collimated to 0.1 mm × 0.1 mm and the diffraction angle was set at $2\theta = 6.56$ degree.

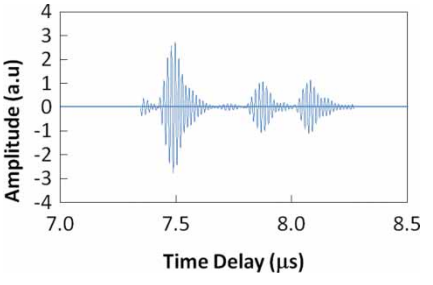

Figure 1. Example of acoustic signals for P wave showing the WC anvil, buffer rod, and sample echoes at 60 MHz.

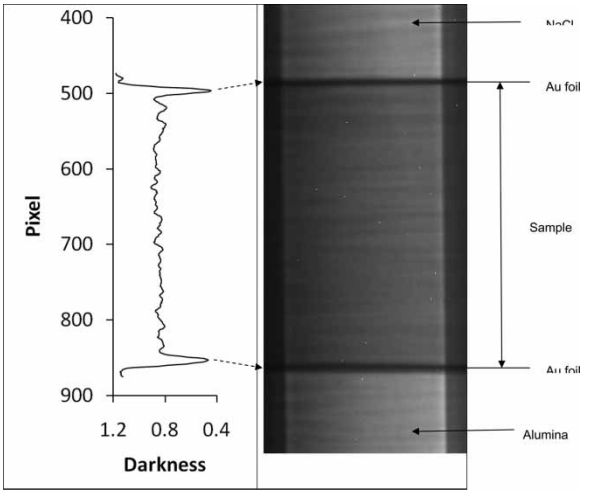

Figure 2. An example of X-radiographic image of the spinel sample recorded at 6 GPa, 573 K (right), and the grey scale readout (left). The two peaks in the pixel- darkness plot correspond to the gold foils defining the top and bottom of the sample.

The unit cell parameters of the sample were refined by six characteristic diffraction lines (220), (311), (222), (400), (331), and (422). The sample temperature was monitored by two W3%Re–W25%Re thermocouples placed next to the sample.

The sample was transformed into single phase of spinel after reaching peak pressure of 7.4 GPa and heating to 1173 K. After that, travel time, sample length, and cell parameters (hence the molar volume and density) were collected along multiple heating/cooling cycles up to 1073 K in the pressure range 0.7–6.5 GPa, from which the compressional and shear wave velocities, elastic longitudinal ($L = \rho V_p^2 = K_s - 4G/3$) and shear moduli ($G = \rho V_s^2$) of Fe_2SiO_4 spinel were derived. The sample was transformed back into fayalite phase by heating it up to 1273 K after collecting data in the last heating cycle.

3. Data analysis

The approach to obtain the pressure and temperature derivatives of elastic moduli using finite strain method has been described in detail in previous publications [9,11–13], which is summarized by the following equations:

$$\rho V_p^2 = (1 - 2\varepsilon)^{3/2}(L_1 - L_2\varepsilon), \tag{1}$$

$$\rho V_p^2 = (1 - 2\varepsilon)^{3/2}(M_1 - M_2\varepsilon), \tag{2}$$

$$L_1 = K_{s0} + 4G_0/3, \tag{3}$$

$$L_2 = 5L_1 - 3K_{s0}(K'_{s0} + 4G'_0/3), \tag{4}$$

$$M_1 = G_0, \tag{5}$$

$$M_2 = 5G_0 - 3K_{s0}G'_0, \tag{6}$$

where $\varepsilon = 0.5[1 - (V_0/V)^{2/3}]$. In this approach, all data were fitted to Equations (1)–(6) along isentropes by assuming that the pressure of each datum was raised along adiabatic compression

Downloaded By: [Whitaker, Matthew L.][State University of New York at Stony Brook] At: 04:07 28 September 2008

Downloaded By: [Whitaker, Matthew L.][State University of New York at Stony Brook] At: 04:07 28 September 2008

with different foot temperature at zero pressure. The following Equations (7)–(11) were used in the fit to constrain the thermoelastic properties at zero pressure:

$$V(0,T) = V(0,298)\exp\left(\int_{298}^{T} \alpha_T \, dT\right) \tag{7}$$

$$K_s(0,T) = K_s(0,298) - (T-298)(\partial K_s/\partial T)_p \tag{8}$$

$$G(0,T) = G(0,298) - (T-298)(\partial G/\partial T)_p \tag{9}$$

$$K'_{ss}(0,T) = (K'_s - (T-298)\left(\frac{\partial^2 K_s}{\partial P \partial T}\right)_p + \left(\frac{\partial K_s}{\partial T}\right)_p (\gamma T/K_s) \tag{10}$$

$$G'_s(0,T) = (G' - (T-298)\left(\frac{\partial^2 G}{\partial P \partial T}\right)_p + \left(\frac{\partial G}{\partial T}\right)_p (\gamma T/K_s) \tag{11}$$

$$P = (1-2\varepsilon)^{s/2}\left[3K_s\varepsilon - (36K_s - 9K_sK'_{ss})\varepsilon^2\right]/2 \tag{12}$$

in which $V_0 = 42.053\,\mathrm{cm}^3/\mathrm{mol}$ from previous diamond anvil cell powder X-ray diffraction [14] and single X-ray diffraction [15] is used. In addition, room pressure thermal expansivity $\alpha_T 2.455 \times 10^{-5} + 3.591 \times 10^{-9}T - 0.3703T^{-2}$ was constrained from the literature [16] based on the experimental data of [17]. These thermal expansion coefficients were compiled in [18,19]. The cross derivatives $(\partial^2 K_s/\partial P \partial T)_p$ and $(\partial^2 G/\partial P \partial T)_p$ were assumed to be zero due to the limited pressure and temperature range of the current data. The Gruneisen parameter γ was constrained by $q = (\partial \ln \gamma/\partial \ln V)_T$ with $q = 1$ (i.e. $\gamma\rho =$ constant), with a mean value of

Table 1. Experimental data of Fe_2SiO_4 spinel.

P (GPa)	T (K)	$2t_P$ (μs)	$2t_S$ (μs)	l (mm)	ρ (g/cm^3)	V_P (km/s)	V_S (km/s)	K_s (GPa)	G (GPa)
3.73	307	0.2083	0.4224	0.842	4.932	8.087	3.989	218.0	78.5
2.43	307	0.2103	0.4260	0.844	4.902	8.025	3.962	213.1	76.9
1.66	307	0.2111	0.4286	0.845	4.884	8.002	3.942	211.6	75.9
0.71	307	0.2123	0.4314	0.847	4.862	7.976	3.926	209.4	74.9
3.85	373	0.2081	0.4262	0.841	4.928	8.085	3.948	219.7	76.8
2.70	373	0.2101	0.4294	0.844	4.901	8.030	3.929	215.2	75.7
2.09	373	0.2115	0.4316	0.845	4.887	7.991	3.916	212.1	74.9
1.17	373	0.2133	0.4348	0.847	4.866	7.943	3.897	208.5	73.9
4.29	473	0.2091	0.4314	0.842	4.928	8.049	3.902	219.2	75.0
3.16	473	0.2113	0.4334	0.844	4.902	7.991	3.896	213.8	74.4
2.51	473	0.2127	0.4358	0.845	4.886	7.941	3.876	210.2	73.4
1.58	473	0.2145	0.4386	0.847	4.864	7.895	3.862	206.5	72.5
4.74	573	0.2099	0.4346	0.842	4.927	8.020	3.874	218.3	73.9
3.54	573	0.2121	0.4368	0.844	4.900	7.961	3.866	212.9	73.2
2.98	573	0.2137	0.4392	0.845	4.886	7.908	3.848	209.1	72.4
2.17	573	0.2155	0.4424	0.846	4.867	7.853	3.825	205.2	71.2
5.18	673	0.2111	0.4372	0.841	4.927	7.972	3.850	215.8	73.0
4.01	673	0.2129	0.4402	0.844	4.900	7.931	3.836	212.1	72.1
3.43	673	0.2145	0.4422	0.845	4.886	7.883	3.824	208.3	71.4
2.61	673	0.2165	0.4456	0.847	4.866	7.822	3.801	204.0	70.3
5.57	773	0.2115	0.4400	0.842	4.925	7.958	3.826	215.8	72.1
4.41	773	0.2137	0.4454	0.845	4.898	7.908	3.795	212.3	70.5
3.86	773	0.2153	0.4456	0.845	4.885	7.848	3.792	207.2	70.3
5.97	873	0.2125	0.4428	0.842	4.923	7.920	3.801	214.0	71.1
4.84	873	0.2149	0.4492	0.845	4.897	7.862	3.762	210.3	69.3
4.19	873	0.2165	0.4480	0.845	4.881	7.802	3.771	204.6	69.4
6.28	973	0.2133	0.4454	0.841	4.920	7.889	3.778	212.5	70.2
5.10	973	0.2153	0.4526	0.844	4.892	7.844	3.732	210.2	68.1
6.49	1073	0.2139	0.4478	0.841	4.914	7.867	3.758	211.6	69.4

Downloaded By: [Whitaker, Matthew L.][State University of New York at Stony Brook] At: 04:07 28 September 2008

1.29–1.30 at ambient conditions [15,17]. With these constraints and assumptions, the results of the elastic properties, including K_s, G, K_s', G', $(\partial K_s/\partial T)_p$, and $(\partial G/\partial T)_p$ were simultaneously refined by a least square fit of the experimental data in the entire pressure and temperature range. An important attribute to note about the current data analysis is that the sample pressure is directly calculated using Equation (12) instead of relying on secondary pressure calibration as those in previous studies.

4. Results and discussions

The details of the experimental P–T conditions, travel times for P and S waves, length of the sample, density calculated from X-ray diffraction data, the calculated velocities, and bulk and shear modulus of the Fe_2SiO_4 spinel are summarized in Table 1. Both the P and S wave velocities for the Fe_2SiO_4 spinel increase systematically with increasing pressure along different isotherms and decrease with increasing temperature at the same pressures (Figure 3). The molar volume from X-ray diffraction shows a systematic decrease upon compression along each isotherm (Figure 4). The calculated bulk and shear moduli from elastic wave velocity and density data are presented in Figure 5.

The velocity and density data measured in the entire P–T range were fitted to the third-order finite strain method as described in the previous section, yielding $K_{s0} = 204.5(7)$ GPa, $G = 73.6(3)$ GPa, $K_s' = 4.3(3)$, $G' = 1.2(1)$, $(\partial K_s/\partial T)_p = -0.027(2)$ GPa/K, and $(\partial G/\partial T)_p = -0.017(1)$ GPa/K. The compressional and shear wave velocities from the current fit are shown as dashed lines along each isotherm (Figure 3), the total root mean square (r.m.s.) misfit between the observed and fitted P and S wave velocities is about 0.01 km/s. An extensive survey of the literature on the room temperature crystal structure data on the spinel phase of Fe_2SiO_4 reveals that the 1 bar room temperature molar volume (V_0) varies from 42.007 to 42.075 cm^3/mol. This

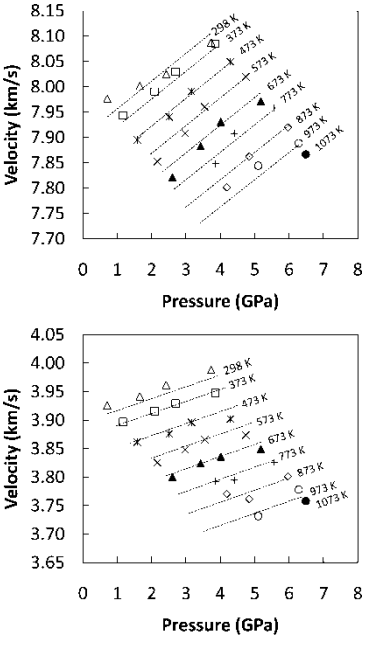

Figure 3. (a) P wave and (b) S wave velocities of Fe_2SiO_4 spinel as a function of sample pressure and temperature. The dashed lines are the calculated P and S wave velocities by finite strain method along experimental isotherms.

Downloaded By: [Whitaker, Matthew L.][State University of New York at Stony Brook] At: 04:07 28 September 2008

Table 2. Elastic moduli of $(Mg,Fe)_2SiO_4$ spinel and their pressure and temperature derivatives.

References	Method*	X_{Fe}	K (GPa)†	dK/dP	G (GPa)	dG/dP	dKs/dT	dG/dT
Chung 1971	US	0	186	4.4	109			
Weidner et al. 1984	BS	0	184		119			
Meng et al. 1994	XRD	0	182 (3)	4.2 (3)			−0.020	
Kiefer et al. 1997	DFT	0	190	4.19	125	1.12		
Matsui 1999	MD	0	181.0 (3)	4.10 (2)	124.2 (5)	1.2 (2)	−0.021	−0.016 (1)
Jackson et al. 2000	BS	0	185 (3)		120 (2)		−0.024 (3)	−0.015 (2)
Li 2003	US	0	185 (2)	4.5 (2)	120 (1)	1.5 (1)		
Higo et al. 2006	US	0	185 (2)	4.4 (2)	127 (1)	1.3 (1)		
Sinogeikin et al. 2001	BS	0.09	188 (3)	4.1 (3)	120 (2)	1.3 (2)	−0.021 (2)	−0.016 (2)
Nishihara et al. 2004[1]	XRD	0.09	187	4.41 (1)			−0.021 (5)	
Mao et al. 1969	XRD	0.1	196 (10)	4-fixed				
Chung 1971	US	0.1	187	4.5	108			
Mao et al. 1969	XRD	0.2	208 (10)	4-fixed				
Chung 1971	US	0.2	189	4.6	107			
Higo et al. 2006	US	0.2	187 (2)	4.4 (2)	116 (1)	1.4 (1)		
Sinogeikin et al. 1997	BS	0.25	193 (3)		113 (2)			
Zerr et al. 1993	XRD	0.4	183 (2)	5.4 (2)				
Chung 1971	US	0.5	193	4.8	102			
Higo et al. 2006	US	0.5	191 (2)	4.4 (2)	102 (1)	1.0 (1)		
Hazen 1993	XRD	0.6	203 (2)	4.8-fixed				
Hazen 1993	XRD	0.8	205 (2)	4.8-fixed				
Mao et al. 1969	XRD	1	211 (10)	4-fixed				
Mizutani et al. 1970	US	1	212					
Liebermann 1970	E	1	199					
Chung 1971	E	1	196	5.1	89			
Akimoto 1972	US	1	205					
Liebermann 1975	US	1	193	4-fixed	75			
Wilburn and Bassett 1976	XRD	1	210 (12)[2]	4-fixed				
Sato 1977	XRD	1	197 (2)	4-fixed				
Finger et al. 1979	XRD	1	196 (6)	4-fixed				
Rigden and Jackson 1991	US	1	201	5.59	79	1.06		
Hazen 1993	XRD	1	207 (3)	4.8-fixed				
This study (finite strain)	US	1	204.5 (7)	4.3 (3)	73.6 (3)	1.2 (1)	−0.027 (2)	-0.017 (1)

*US, ultrasonic interferometry; BS, Brillouin scattering spectroscopy; XRD, static compression X-ray diffraction; DFT, density function theory; MD, molecular dynamics simultation; E, estimated from systematic relations.
†K_T and K'_T for XRD and MD, K_s and K'_s for US, BS, E, and DFT. Conversion equations: $K_s = K_T(1+\alpha\gamma T)$, $K'_T = [K'_s + q\alpha\gamma T - \gamma T(\partial K_T/\partial T)/K_T]/(1+\alpha\gamma T)$, $(\partial K_s/\partial T)_p = (1+\alpha\gamma T)(\partial K_T/\partial T)_p + K_T[\alpha\gamma + \alpha^2\gamma T + \gamma T(\partial\alpha/\partial T)]$, where $q = (\partial \ln\gamma/\partial \ln V)_T$ is the volume dependence of γ. To be consistent with the current study, it is assumed that $q = 1$.
[1]Fitted with fixed $V_0 = 527.83$ A and $K_{T0} = 187$.
[2]Corrected value fitted by least square using the original data.

difference (∼0.16%) in V_0 only causes a variation of 0.3%, 0.2%, 0.08%, 0.1%, 0.4%, 0.2% in the fitting results of K_s, G, K'_s, G', $(\partial K_s/\partial T)_p$, and $(\partial G/\partial T)_p$ respectively, which are within the current experimental and fitting errors. As shown in Table 2, both the bulk and shear moduli for Fe_2SiO_4 spinel derived from this study are consistent with those from X-ray diffraction study ($K_s = 196-211$) [14,15,20,21], systematic estimation ($K_s = 196-199$) [22,23], and ultrasonic studies ($K_s = 193-212$; $G = 75-79$) [24–27] within the claimed uncertainties. The only exception is that the shear modulus from the estimation ($G = 89$, [23]) is ∼21% higher compared with our result ($G = 73.6$).

Our elastic property results were compared with those from the literature [1–8,15–17,20–32] on the spinel phase of Mg_2SiO_4–Fe_2SiO_4 solid solution in order to evaluate the effect of Fe content on elastic properties (Table 2). Since the adiabatic and isothermal values for bulk modulus and its pressure derivative at ambient conditions differ by less than 1%, which is often within the reported experimental error, the results from ultrasonic and Brillouin scattering studies (adiabatic) and those from X-ray diffraction studies (isothermal values) are therefore listed as general terms

Downloaded By: [Whitaker, Matthew L.][State University of New York at Stony Brook] At: 04:07 28 September 2008

as K and K'. However, the difference for the temperature derivative of bulk modulus is not negligible, it is necessary to convert all the literature values to either adiabatic or isothermal values for comparison of this property. In Table 2, all the temperature derivatives of bulk modulus are converted to $(\partial K_s/\partial T)_p$.

The bulk modulus of $(Mg,Fe)_2SiO_4$ spinel increases slightly from 184 to ~205 with increasing Fe content from 0 to 100%, whereas the shear modulus decreases significantly from 125 to 74 in the same range of composition. Therefore, the shear modulus shows a stronger dependence on Fe content than the bulk modulus. The pressure and temperature dependence of the bulk and shear moduli remain essentially constant with average value of 4.2–4.4, 1.2–1.3, −0.024 GPa/K, and −0.016 GPa/K for K_s', G', $(\partial K_s/\partial T)_p$, and $(\partial G/\partial T)_p$, respectively (Table 2). Examination of the bulk and shear modulus show that data from different studies are still scattered, especially for the pure Fe_2SiO_4 spinel end member (Figure 4). Combining all the elastic moduli data on

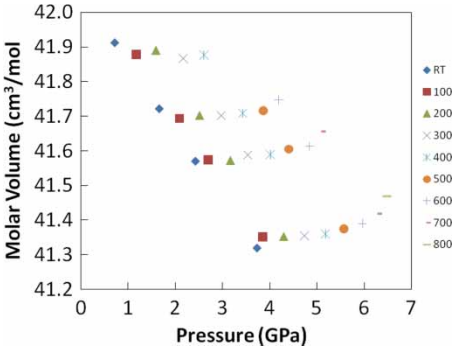

Figure 4. Molar volume of Fe_2SiO_4 spinel as a function of pressure and temperature.

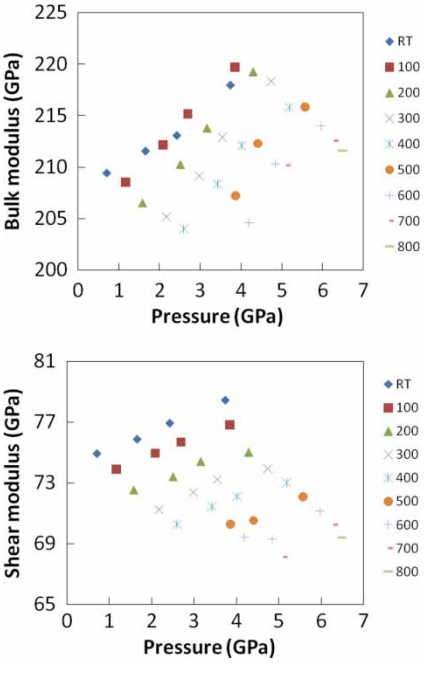

Figure 5. Elastic moduli of Fe_2SiO_4 spinel as a function of pressure and temperature: (a) bulk modulus and (b) shear modulus. Lines are guidelines for different isotherms.

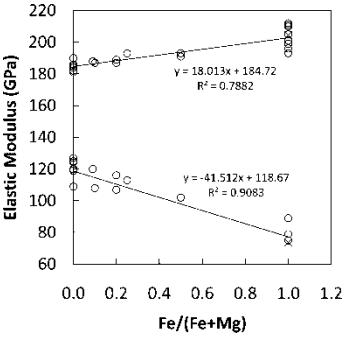

Figure 6. Bulk and shear moduli of $\gamma(Mg,Fe)_2SiO_4$ spinel vary as a function of iron content. Open circles refer to literature data; crosses refer to data from this study. The two solid lines are linear fitting (equations shown) of all the ultrasonic studies from the literature together with our data for the bulk and shear moduli, respectively.

ringwoodite obtained by using ultrasonic interferometry with those from the current study yields the following relationship for the dependence of the elastic moduli on iron content: $K_s = 184.7 + 18.1\,X_{Fe}$, and $G = 118.7 - 41.4\,X_{Fe}$. The use of only ultrasonic data is to keep internal consistency with the same technique with the assumption that the sample qualities used in these studies are comparable. As noted in [1], slightly different trends of the variation of elastic moduli as a function of iron content may result when data from different techniques are used. The ambiguity is partly due to the poor coverage of the composition range on iron-bearing ringwoodite, especially those with more than 50% of iron content, which points to a direction where further studies in these compositions are required in order to better constrain the effect of iron content on the bulk and shear moduli.

Acknowledgements

The authors thank Dr. Donald Lindsley for providing the fayalite sample powder. They also thank the editor and the reviewers who helped improve the manuscript. This project was supported by NSF grant to B. Li (EAR0635860). The experiment was conducted at X17B2 of NSLS, Brookhaven National Laboratory which is supported by the U.S. Department of Energy, Office of Science, Office of Basic Energy Sciences, under contract no. DE-AC02-98CH10886 and by COMPRES, the Consortium for Materials Properties Research in Earth Sciences under NSF Cooperative Agreement EAR 06-49658, Mineral Physics Institute Publication No. 469.

References

[1] Y. Higo, T. Inoue, B. Li et al., Phys. Earth Planet. Int. 159 (2006), pp. 276–285.
[2] B. Li, Am. Miner. 88 (2003), pp. 1312–1317.
[3] J.M. Jackson, S.V. Sinogeikin, and J.D. Bass, Am. Miner. 85 (2000), pp. 296–303.
[4] Y. Meng, Y. Fei, D.J. Weidner et al., Phys. Chem. Miner. 21 (1994), pp. 407–412.
[5] S.M. Rigden, G.D. Gwanmesia, J.D.F. Gerald et al., Nature 354 (1991), pp. 143–145.
[6] D.J. Weidner, H. Sawamoto, S. Sasaki et al., J. Geophys. Res. 89 (1984), pp. 7852–7860.
[7] M. Matsui, Phys. Earth Planet. Int. 116 (1999), pp. 9–18.
[8] B. Kiefer and L. Stixrude, Geophys. Res. Lett. 24 (1997), pp. 2841–2844.
[9] B. Li, J. Kung, and R.C. Liebermann, Phys. Earth Planet. Inter. 143–144 (2004), pp. 559–574.
[10] B. Li, K. Chen, J. Kung et al., J. Phys. Condens. Matter 14 (2002), pp. 11337–11342.
[11] G.F. Davis and A.M. Zziewonski, Phys. Earth Planet. Inter. 10 (1975), pp. 336–343.
[12] B. Li and J. Zhang, Phys. Earth Planet. Inter. 151 (2005), pp. 143–154.
[13] W. Liu, J. Kung, and B. Li, Geophys. Res. Lett. 32 (2005), pp. L16301.
[14] D.R. Wilburn and W.A. Bassett, High Temp. – High Press. 8 (1976), pp. 343–348.
[15] L.W. Finger, R.M. Hazen, and T. Yagi, Am. Miner. 64 (1979), pp. 1002–1009.
[16] I. Suzuki, E. Ohtani, and M. Kumazawa, J. Phys. Earth, 27 (1979) pp. 53–61.
[17] H.K. Mao, T. Takahashi, W.A. Bassett et al., J. Geophys. Res. 74 (1969) pp. 1061–1069.

Downloaded By: [Whitaker, Matthew L.][State University of New York at Stony Brook] At: 04:07 28 September 2008

[18] H. Watanabe, *Thermochemical properties of synthetic high-pressure compounds relevant to the Earth's mantle*, in *High Pressure Research in Geophysics*, S. Akimoto and M.H. Manghnani, eds., Center for Academic Publication, Tokyo, 1982, pp. 441–464.
[19] Y. Fei and S.K. Saxena, Phys. Chem. Miner. 13 (1986), pp. 311–324.
[20] Y. Sato, *Equation of state of mantle minerals determined through high-pressure X-ray study*, in *High Pressure Research, Applications in Geophysics*, M.H. Manghnani and S. Akimoto, eds., Academic Press, New York, 1977, pp. 307–323.
[21] R.M. Hazen, Science 259 (1993), pp. 206–209.
[22] R.C. Liebermann, J. Geophys. Res. 75 (1970), pp. 4029–4034.
[23] D.H. Chung, Geophys. J. R. Astr. Soc. 25 (1971), pp. 511–538.
[24] S.M. Rigden and I. Jackson, J. Geophys. Res. 96 (1991), pp. 9999–10006.
[25] R.C. Liebermann, Geophys. J. R. Astr. Soc. 42 (1975), pp. 899–929.
[26] S. Akimoto, Tectophysics, 13 (1972), pp. 161–187.
[27] H. Mizutani, Y. Hamano, Y. Ida, et al., J. Geophys. Res. 75 (1970), pp. 2741–2747.
[28] S.V. Sinogeikin and J.D. Bass, Geophys. Res. Lett. 24 (1997), pp. 3265–3268.
[29] S.V. Sinogeikin, T. Katsura, and J.D. Bass, J. Geophys. Res. 103 (1998), pp. 20819–20825.
[30] S.V. Sinogeikin, J.D. Bass, and T. Katsura, Geophys. Res. Lett. 28 (2001), pp. 4335–4338.
[31] A. Zerr, H.R. Reichmann, H. Euler, et al., Phys. Chem. Miner. 19 (1993), pp. 507–509.
[32] Y. Nishihara, E. Takahashi, K.N. Matsukage, et al., Phys. Earth Planet. Inter. 143–144 (2004), pp. 33–46.

Downloaded By: [Whitaker, Matthew L.][State University of New York at Stony Brook] At: 04:07 28 September 2008